Journal of Materials Research and Technology 36 (2025) 4020–4030

Contents lists available at ScienceDirect

Journal of Materials Research and Technology

journal homepage: www.elsevier.com/locate/jmrt

Investigation of the influence of thermal overloads on mechanical properties of S500 high-strength structural steel using electromagnetic testing technology

René Gansel [a,*], Moritz Braun [b,c], Sören Ehlers [b,c], Sebastian Barton [a]

[a] Institut für Werkstoffkunde (Materials Science), Leibniz Universität Hannover, Garbsen, Germany
[b] Institut für Maritime Energiesysteme (Maritime Energy Systems), Deutsches Zentrum für Luft- und Raumfahrt (DLR), Geesthacht, Germany
[c] Institut für Konstruktion und Festigkeit von Schiffen (Ship Structural Design and Analysis), Technische Universität Hamburg, Hamburg, Germany

ARTICLE INFO

Keywords:
Fatigue strength
Heat treatment
Non-destructive testing
Eddy current testing
High-strength steel

ABSTRACT

High-strength steels are mostly realized via a very fine-grained microstructure by a thermomechanical manufacturing process. If the temperature of the steels exceeds a critical range, e.g., due to a fire or inappropriate flame straightening, coarse grain formation, and thus local damage in the form of softening of the structure can occur. This results in a lower fatigue strength. Currently, there is no possibility to inspect the mechanical properties directly on the structure after thermal exposure.

To investigate the influence of thermal overloads on mechanical properties and the qualification of non-destructive electromagnetic testing technology for the detection of thermal damage, tensile and fatigue specimens of S500G1+M high-strength structural steel were subjected to different heat treatments in a preheated chamber furnace at temperatures of 550, 1000 and 1300 °C. The resulting changes in microstructure, hardness, yield strength, tensile strength, elastic modulus, fatigue strength and electromagnetic signals were compared to the initial state. The combined results show that thermal damage leading to a degradation of the mechanical properties can be detected using harmonic analysis of eddy current signals. Referencing the initial state in the impedance plane of the third harmonic, a deviation can be detected directly on the component or structure using rapid and non-destructive testing, thus indicating a change in the fatigue strength. In addition, the amplitudes of the first and third harmonics show an inverse correlation to hardness, yield strength and tensile strength.

Nomenclature:

HSS	High-strength steel
HA-EC	Harmonic analysis of eddy current signals
TMCR	Thermomechanical-controlled rolling

1. Introduction

High-strength steel (HSS) is indispensable in certain applications. A defined microstructure is crucial in this respect, but thermal loads can alter this state. Thermal overloads can be related to different causes, e.g., fire, thermal loads during service, or due to processes like flame straightening. For instance, fire is recognized as a significant hazard that can occur during the service life of a structure. The use of inappropriate construction materials and structural systems has been shown to have devastating consequences during a fire event. Therefore, maintaining structural integrity during fire is a safety requirement in the design of structures. Flame straightening is used in shipbuilding, for example, to reduce shape deviations in sheets. If the flame straightening temperature exceeds a certain thermal limit, localized damage can occur in the form of softening of the component.

The resulting microstructure after thermal overload is often unknown. Studies have shown that various high-strength steels exhibit significantly reduced mechanical properties after thermal exposures above 600–700 °C, see for example [1–5]. As a result, previously calculated or tested strengths and fatigue strengths become obsolete. Instead, it is necessary to determine the current actual state. Mobile and time-efficient, non-destructive testing that is sensitive to changes in the microstructure is required.

* Corresponding author. Institut für Werkstoffkunde (Materials Science), Leibniz Universität Hannover, An der Universität 2, D-30823, Garbsen, Germany.
E-mail address: gansel@iw.uni-hannover.de (R. Gansel).

https://doi.org/10.1016/j.jmrt.2025.04.121
Received 27 January 2025; Received in revised form 10 April 2025; Accepted 12 April 2025
Available online 12 April 2025

The aim of this feasibility study was to determine if a critical thermal load that degrades the mechanical properties can be identified on an exemplary S500M high-strength structural steel using harmonic analysis of eddy current (HA-EC) signals. This question has not been systematically addressed in the open literature for high-strength steels in general. The S500M steel is increasingly being used in steel structures, hydraulic steel structures, mechanical engineering and storage tanks where high weldability is required despite the use of high-strength steels. To investigate the effect of heat treatments on the mechanical properties and to be able to analyse the relationship between microstructure, mechanical properties and non-destructively obtained measurement data, specimens were examined metallographically after heat treatment. The mechanical properties were determined by means of tensile tests and vibration tests.

2. Influence of thermal exposure on mechanical properties of structural steels

Thermal overloads refer to the exposure of materials to high temperatures, either in a sustained manner or through thermal cycling, which can cause thermal fatigue, creep or microstructural changes and lead to premature failure. Thermal exposure and in particular thermal overloads can be related to different causes, e.g., fire, thermal loads during service, or due to processes like flame straightening. When steel is subjected to high temperatures, it can experience a number of changes in its microstructure and mechanical properties (i.e., strength, ductility, toughness, and fatigue strength). These changes can include the growth of grain size, precipitation of brittle phases, and the reduction of ductility due to a loss of dislocation mobility [6].

One of the most critical ways that thermal overloads affect the mechanical properties of steel is through the formation of cracks and defects. These defects can propagate and lead to fracture, reducing the overall ductility and toughness of the material [7]. The severity of these defects is largely dependent on the cooling rate, which can affect the size and shape of the grains and the distribution of precipitates [8].

Research has shown that the ductility and toughness of steel can also be influenced by the heating rate, duration, and temperature. High heating rates can cause rapid thermal expansion, leading to thermal shock and increased susceptibility to brittle fracture [9]. Similarly, prolonged exposure to high temperatures can cause the formation of brittle phases, leading to reduced ductility and toughness [10].

2.1. Microstructure of high-strength structural steels

High-strength structural steels are a group of alloys that offer improved mechanical properties compared to carbon steel. They achieve these properties by developing specific microstructures through controlled thermomechanical processing. The resulting microstructure can be adjusted to reach optimal properties such as strength, hardness, ductility, and toughness. These properties are achieved through a combination of specific alloying elements and heat treatment. HSS commonly use thermomechanical-controlled rolling or quenching and tempering to produce microstructures with high strengths, as well as multiphase microstructures that balance strength and ductility.

Thermomechanical-controlled rolling (TMCR) is a technique that can be used to produce high-strength structural steels. This process involves using a combination of temperature, strain rate and deformations to achieve the desired mechanical properties in the final product. The process comprises of a series of steps including heating the steel to a suitable temperature to facilitate full austenite transformation, followed by controlled rolling under the desired temperature and strain rate. The steel is then cooled uniformly using a temperature and cooling rate that has been optimized for the specific application.

One of the advantages of TMCR is its ability to produce uniform microstructure, minimizing the need for expensive microstructural alterations during the post-processing stage. Additionally, TMCR can be used to control the ferrite grain size and distribution, resulting in a microstructure that promotes toughness, ductility, and impact resistance within the alloy [11]. The typical microstructure of TMCR steel can vary depending on the specific processing parameters used; however, in general, the microstructure of structural steel produced by TMCR is characterized by a fine-grained ferrite and pearlite microstructure. This microstructure is often uniform and highly refined, leading to improved mechanical properties. TMCR can also promote the formation of other microstructural features, such as bainitic ferrite, which can further enhance the properties of the steel [12].

2.2. Effect of thermal exposure on ductility and toughness of steels

The specific effects of thermal overloads on the ductility and toughness of steel can vary depending on the composition and microstructure of the material. For example, HSS alloys can be more susceptible to embrittlement due to the formation of brittle intermetallic phases at high temperatures [13]. On the other hand, low-carbon steels may experience improved toughness due to the formation of a tough and ductile bainitic microstructure [6].

In summary, thermal overloads can significantly affect the ductility and toughness of steel, leading to increased risk of failure. The severity of these effects is dependent on a variety of factors, including the cooling rate, heating rate, duration, and temperature, as well as the composition and microstructure of the steel.

A recent study by *Wang* et al. [14] revealed that thermal cracks normally initiate and propagate along the oxidized grain boundaries of low-alloy steel; nevertheless, crack propagation is restricted by the fine precipitates and lath structure of martensite.

There has been much research on deterioration of mechanical properties of structural steels at elevated temperatures in the context of fire-safe design, see e.g., Refs. [15–17] or [18]. In principle, mechanical properties decrease steadily with increasing temperature. Slowly at temperatures between room temperature and about 200 °C and more rapidly at higher temperatures [17].

Similarly, the mechanical performance of structural steels has been studied after exposure to high temperatures and subsequent air cooling to room temperature as a simulation of post-fire conditions. For instance, *Saedi Daryan* et al. [1] investigated the stress-strain behaviour of S235 steel after the exposure of varying temperature cycles between 25 and 900 °C. Similar tests were performed by *Kang* et al. [2] for a Q460 steel up to 900 °C, by *Zeybek* et al. [3] for S700MC steel up to 1200 °C, by *Pandey and Young* [19] for 900MH and 960MH up to 900 °C and by *Qiang* et al. [4] for S460 and S690 steel after the exposure to temperatures up to 1000 °C. It is found that the mechanical properties of HSS are significantly affected by the exposure to high temperatures. For S460 and S690 steel, a reduction in mechanical properties is observed for temperatures above 600 °C [4], and for S700MC steel also above 600 °C [3]. *Wang* et al. [5] showed that after heat treatment at 700 °C, the yield stress of the quenched and tempered high-strength steel Bisalloy80 is reduced by an average of 37% and of Bisalloy400 by 61%. For ultra-high-strength steels, this transition temperature is found at lower temperatures, e.g., 300 °C for Grade 1200 steel [20].

The effect of flame straightening on the mechanical properties of steels is a matter of debate and depends on several factors like the type of steel and the degree of straightening. Some studies have suggested that flame straightening can have detrimental effects on the mechanical properties of steel [21], including reduced toughness and increased susceptibility to fatigue crack growth in the affected areas. However, other studies have reported that mechanical properties are not affected, or even improved, e.g., by flame straightening. Assessing the effect of flame straightening on microstructural, mechanical and fracture properties of S235JR, S460ML and S690QL structural steels, *Lacalle* et al. [22] came to the conclusion that it is not possible to establish general recommendations for flame straightening processes. It is, therefore, essential to note that any heat-based straightening method could

potentially reduce the material properties of a steel structure. This is typically related to microstructural changes that are caused by either to high temperatures (in a similar range as previously stated) or due to rapid cooling.

In large engineering structures like ships, flame straightening is often performed by a combination of a torch to heat the plate on spots or along lines and water spraying for cooling at other locations. Due to constrains during heat expansion and shrinkage in previously expanded regions, a distribution of residual stresses is created, which leads to the desired permanent deformation [23]. Clearly, spraying water onto a hot steel plate can cause significant cooling rates. It thus needs to be controlled to avoid the formation of martensite. In addition, in order to prevent the formation of tertiary cementite in low carbon ferritic-pearlitic steels, cooling times longer than 100 s between 400 and 600 °C should also be avoided [22]. It is typically recommended to avoid temperatures above 600–650 °C during flame straightening due to the aforementioned effects on mechanical properties, see Ref. [24]. *Gyura* et al. [21] showed in a systematic investigation that hardness and Charpy V-notch impact toughness may be significantly reduced for heating temperatures above 800 °C and rapid water cooling. While the effect on a mild S355J2 steel was limited, the effect became more pronounced for XAR400 and S960QL steel.

In general, there is plenty of research on mechanical behaviour of steels at high temperatures or after thermal overloads; however, the investigations of the effect of thermal overloads in combination with cooling rates achieved, e.g., during flame straightening are rare. Thus, further research is needed to fully understand and mitigate these effects in order to improve the performance and reliability of steel components subjected to thermal overloads.

2.3. *Effect of thermal exposure on fatigue strength*

Thermal exposure and thermal overloads can have a significant impact on the fatigue strength of steels. In general, thermal overloads tend to reduce the fatigue strength of a material. This is because they can introduce microstructural changes in the material that can lead to crack initiation and propagation. The extent of the reduction in fatigue strength depends on several factors, including the magnitude and duration of the thermal overload, the material's composition and microstructure, and the loading conditions the material experiences, c.f [6,7,9].

One of the primary mechanisms through which thermal overloads reduce fatigue strength is by inducing residual stresses in the material. These stresses can result from thermal expansion or contraction, or from differential cooling rates across the material. Residual stresses can create microstructural changes in the material that make it more susceptible to cracking. In addition, thermal overloads can lead to changes in the material's grain structure, including grain growth or recrystallization. These changes can alter the material's fatigue properties and reduce its overall strength.

Another factor that can influence the impact of thermal overloads on fatigue strength is the material's temperature sensitivity. Some materials are more sensitive to changes in temperature than others, meaning that they are more prone to microstructural changes or cracking under thermal overloads. The loading conditions the material experiences can also affect its fatigue strength under thermal overloads. For example, materials that undergo cyclic loading at high stress levels are more susceptible to cracking than those that experience lower stress levels [25].

The influence of thermal overloads on the fatigue strength of materials has been studied mainly for low-cycle fatigue properties [26–28]. The effect of thermal overloads on fatigue strength depends on several factors, including the material's composition, microstructure, and thermal history. For instance, materials with high thermal conductivity and low thermal expansion coefficients tend to be more resistant to thermal fatigue than materials with low thermal conductivity [29].

Furthermore, the severity of the thermal overload, including the temperature and duration of exposure, also plays a significant role in determining the fatigue strength reduction. In general, as the temperature and duration of exposure increase, the fatigue strength of materials decreases [30].

Several mechanisms have been proposed to explain the reduction in fatigue strength due to thermal overloads, including microstructural changes such as grain growth, precipitation, and phase transformations, as well as the formation of cracks and defects.

Various testing methods, such as thermal cycling fatigue tests, have been developed to study the effect of constant thermal loads on fatigue strength. Additionally, predictive models, such as the Coffin-Manson equation [31] and the Smith-Watson-Topper model [32], have been developed to estimate the fatigue life of materials under thermal loads. However, the effects of short-term and unexpected thermal overloads, e.g. due to fire or improper flame straightening, on fatigue strength have not been adequately investigated, as in practice this can only be done by destructive testing.

The only study that investigated the effect of thermal overloads and rapid cooling was performed by *Guo* et al. [33] for post-fire hysteretic and low-cycle fatigue behaviours of Q345 carbon steel. Their test results showed that water cooling with a rapid cooling speed from temperatures of 750 °C or 1000 °C have a significant impact on the cyclic behaviour of the Q345 steel. They related this effect to the formation of martensite during cooling, which results in a decrease in the ductility and a sharp reduction of the fatigue life.

In conclusion, the influence of thermal overloads on the fatigue strength of materials is a complex phenomenon that depends on several factors. The main problem in predicting the effect of thermal exposure on fatigue strength lies within the determination of the actual temperatures reached and the cooling times, as these are the two parameters that mainly influence microstructural changes. As these parameters are not known after unexpected thermal damage, it is not possible to make a reliable prediction of the remaining service life. Non-destructive testing directly on the respective structure as a tool for assessing thermal damage can therefore provide a solution.

3. Characterization of microstructure using electromagnetic testing

Besides mechanical material properties, thermal overload also affects electrical and magnetic material properties. This can be captured by non-destructive, electromagnetic testing techniques. The harmonic analysis of eddy current signals is a powerful method for characterizing the mechanical properties of ferromagnetic materials, especially steels. This technique is based on the generation and detection of eddy currents, which are produced by electromagnetic induction in conductive materials. The higher the magnetic permeability and electrical conductivity of the material, and the higher the test frequency, the lower the penetration depth of the eddy currents. The basic structure of an eddy current sensor consists of an exciter coil, which generates an alternating magnetic field, and a receiver coil, which detects the changes in the magnetic field caused by the induced eddy currents. The measured signals contain information about the electrical conductivity and the magnetic properties of the material [34].

During harmonic analysis, the measured eddy current signals are broken down with a Fast-Fourier-Transformation into their frequency components. The result of this transformation provides amplitude and phase values, or real and imaginary parts, of the harmonics contained in the measurement signal. These are odd multiples of the test frequency due to the non-linear transmission behaviour or rather the magnetic hysteresis. It also enables a detailed analysis of the signal characteristics and the identification of harmonic frequencies that are influenced by various material properties. Analysing the harmonic components provides valuable information about stresses, hardness, impurities and other mechanical properties of the steel. A key advantage of harmonic

analysis is its ability to perform non-invasive and fast tests. For instance, harmonic analysis of eddy current signals can be used to characterize and differentiate the microstructure and stress distribution in the material [35–38].

This technique is also used to analyse the effects of heat treatments and mechanical stresses on material properties. For instance, the phase transformation of ferrite, martensite and bainite during cooling from the austenite region can be sensitively detected. In addition, changes in the microstructure can be detected as a result of tempering processes [39–43]. It is also possible to correlate mechanical properties such as hardness with characteristic values from the harmonic analysis [44–46]. The data obtained are of great importance for the development of new steel alloys and the optimisation of manufacturing processes. The harmonic analysis of eddy current signals therefore makes an important contribution to improving materials science and materials engineering.

4. Materials and methods

4.1. Specimen preparation and heat treatment

The specimens for the tensile tests and vibration tests were cut out of a rolled S500G1+M sheet ($t = 10$ mm) using water jet cutting. The sides of the test area of the specimens were milled in order to reduce the roughness and generally improve the surface quality. No further surface treatment was carried out. The geometries can be seen in Figs. 2 and 3. The specimens were then heat-treated in a THERMCONCEPT KM 10/13 chamber furnace in furnace atmosphere. The chamber furnace has a thermocouple and temperature control to ensure the required temperature is guaranteed. All specimens were subjected to simultaneous heating and cooling, depending on the specific heat treatment, to ensure the comparability of the results. The heat treatments differed in temperature, duration and type of cooling. The parameters and the respective number of specimens can be found in Table 1. The aim of the heat treatment tests was to achieve a wide range of different microstructures.

In order to achieve a more precise classification of the heat treatments in terms of the resulting temperature in the relevant near-surface area of the vibration specimens, a type K thermocouple was inserted into a bore with a diameter of 1.5 mm and a depth of 2 mm in the centre of an exemplary vibration specimen. This procedure enabled the respective time-temperature curve to be recorded in order to determine the near-surface specimen temperature, particularly for short heat treatment times of 2 min. The corresponding curves for 550, 1000 and 1300 °C are shown in Fig. 1.

As demonstrated in Fig. 1, the near-surface area of the vibration specimen exhibited a temperature of 520 °C after 10 min at 550 °C chamber furnace temperature, 1021 °C at 1000 °C chamber furnace temperature, and 1311 °C at 1300 °C chamber furnace temperature.

Table 1
Heat treatments and number of specimens used.

Heat treatment	Temperature, °C	Time, min	Cooling	Specimens for tensile tests	Specimens for vibration tests
1A	As delivered	–	–	1	3
1B	550	10	Free convection	1	3
1C	1000	10	Free convection	1	3
1D	1300	10	Free convection	1	2
2B	1000	2	Free convection	1	3
2C	1300	2	Free convection	1	2
3B	1300	10	Quenching	1	2

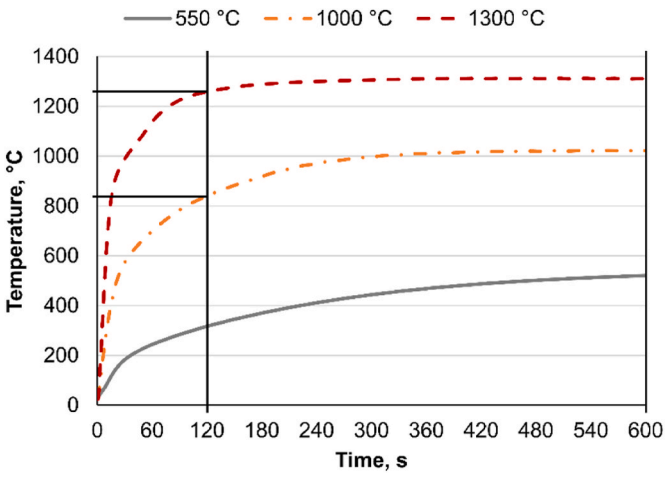

Fig. 1. Temperature curve of the near-surface area of an exemplary vibration specimen for the heat treatment temperatures 550, 1000 and 1300 °C.

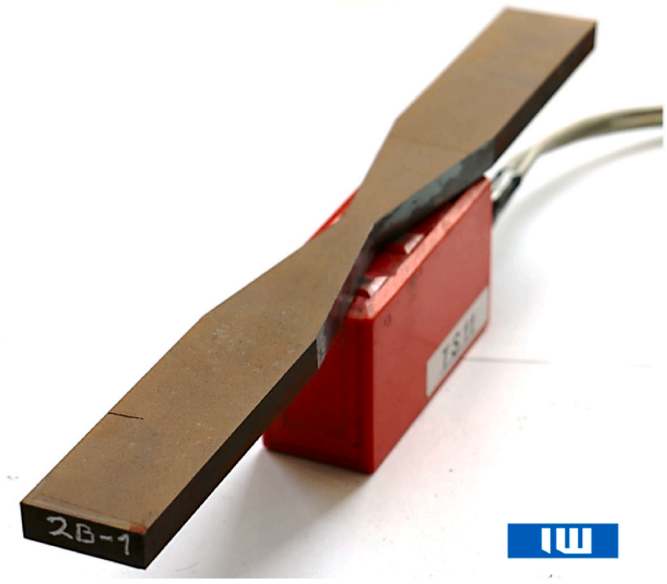

Fig. 2. HA-EC-Sensor used and fatigue test specimen 2B

Thus, it was observed that the lowest chamber furnace temperature did not result in the target temperature being reached within 10 min of the surface-area. On the other hand, the higher chamber furnace temperatures were exceeded because the chamber furnace lost temperature when the specimens were inserted and had to be reheated. It is important to note that the system is inert, meaning that slightly higher chamber furnace temperatures are only reached for a brief period. Additionally, the observed deviation may be due to the accuracy of the two different thermocouples.

Furthermore, after a heat treatment time of 2 min, the near-surface temperature reached 840 °C at 1000 °C chamber furnace temperature and 1259 °C at 1300 °C chamber furnace temperature. Consequently, divergent maximum temperatures and holding times could be achieved using these heat treatments, thus leading to the realization of differing thermal damage.

4.2. Electromagnetic characterization with harmonic analysis of eddy current signals

The testing system used was developed in-house. It consisted of a PC

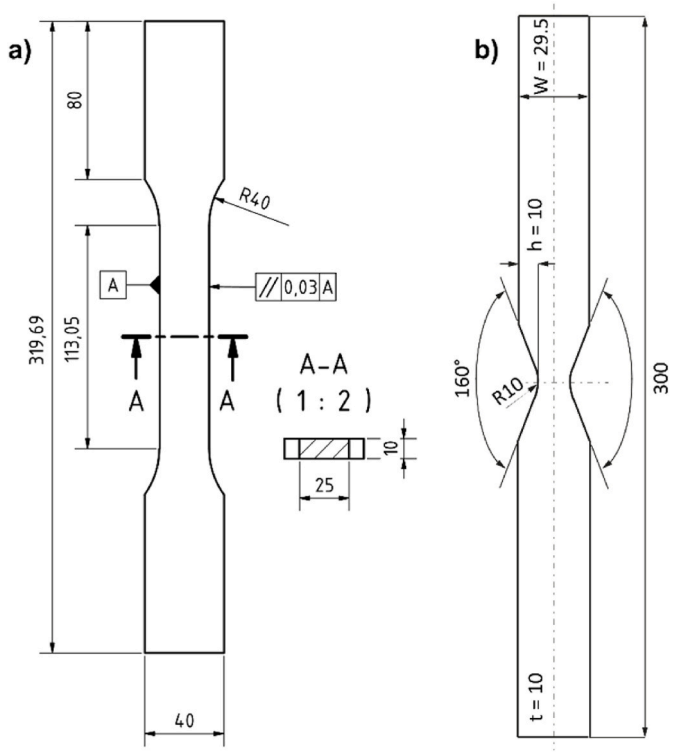

Fig. 3. Schematic illustration of a) the tensile test specimen geometry and b) the fatigue test specimen geometry.

with a measuring card, a power amplifier and a tactile sensor. The sensor shown in the illustration was operated at a test frequency of 3200 Hz with an excitation current of 0.5 A. This test frequency examines the area close to the surface. For the measurement, the specimens were positioned 10 times with the test area on the measuring spot of the sensor to include positioning effects. A potentially existing scale layer was not removed for the test. The same test setup was used for the tensile specimens and the fatigue specimens.

4.3. Mechanical characterization

Tensile testing at room temperature was performed under quasi-static conditions according to ISO 6892-1 [47] in a Zwick Roell Z250 test machine with makroXtens II type P. For this purpose, standard tensile tests with the typical specimen size of $t = 10$ mm and $b = 25$ mm and extensometer gauge length of 71.5 mm were machined. The tensile test specimen geometry is presented in Fig. 3a).

The fatigue tests were carried out under force-controlled tension loading on a Schenk resonance fatigue testing machine equipped with hydraulic clamps with a stress ratio $R = \sigma_{min}/\sigma_{max} = 0$ and at a test frequency of around 32 Hz. The stress amplitudes were determined based on the static material properties. However, it was not possible to conduct testing at the same stress amplitudes due to significant changes in material properties. Tests exceeding 10 million cycles were terminated and classified as run-outs. The fatigue test specimen geometry is presented in Fig. 3b). In order to prevent failure in the clamping area, a notched specimen geometry was used with a stress concentration factor of 1.44 obtained from finite element simulations, see Ref. [48].

4.4. Microstructure characterization

To visualise changes in the microstructure, Klemm III colour etching was used for the micrographs. Additionally, Adler and HNO_3 etching was conducted. However, the Klemm III etching exhibited the most pronounced microstructural differences. The metallographic specimens were taken a few millimetres from the fracture surface of the fatigue test specimens. The fatigue fracture consistently occurred approximately in the centre of the specimens. The micrographs, taken using an optical microscope, were obtained from the surface area of the specimen, which was freely exposed to the furnace atmosphere during the heat treatment.

In addition to the colour etching of the different microstructures, microhardness tests according to Vickers and standard DIN EN ISO 6507 were carried out on the same metallographic specimens. The first indentation was positioned as close as possible to the surface with a distance of 0.2 mm. The indentations were then made automatically in a vertical direction from the top to the bottom of the specimen in 0.2 mm increments. The hardness curve across the specimen was analyzed in order to investigate the homogeneity of the heat treatment, particularly in the case of short heat treatment times. Due to the small differences in the hardness curve, a mean value in HV0.5 including the standard deviation was calculated.

5. Results and discussion

5.1. Metallographic analysis of microstructural changes

The micrographs shown in Fig. 4 were etched with a Klemm III solution. The Vickers microhardness tests were carried out vertically along the microsection surface.

Fig. 4a) shows a ferritic-pearlitic microstructure with minimal proportions of grain boundary cementite in the initial state of S500G1+M. The ferrite grains here have a white to light brown and in the following a blue colour. The dark brown and purple etched grains, on the other hand, are pearlitic and show ferritic grains with linear cementite structures, whereby the typical lamellar morphology is recognisable.

In Fig. 4b), the heat treatment at 550 °C results in a higher proportion of lamellar pearlitic grains and grain boundary cementite compared to the initial state, which simultaneously increases the hardness by 24 HV0.5.

In Fig. 4c), the heat treatment at 1000 °C generally results in disordered grain growth and a lower proportion of cementite, which reduces the hardness to a minimum of 199 HV0.5. In Fig. 4d), the coalescence of smaller grains into significantly larger grains can also be observed.

In Fig. 4e), the short-term heat treatment has resulted in a finer-grained microstructure compared to the initial state, whereby the pearlitic content and the proportion of cementite have increased. This is also reflected in the hardness of 249 HV0.5.

In Fig. 4f), grain growth can be seen due to the higher temperature than in Fig. 4e), resulting in a low hardness similar to the heat treatment in Fig. 4c).

A different microstructure is seen in Fig. 4g) and also a significantly higher hardness is seen here due to the quenching process in water. This resulted in a needle-like martensitic microstructure at room temperature with a hardness of 347 HV0.5. Due to the low carbon content of 0.06 wt.-%, the hardness is lower for a martensitic structure.

5.2. Comparison of mechanical properties in tensile tests

The specimens were characterized by means of tensile testing. The results of each test are presented in Figs. 5 and 6 a comparison of all tests is presented.

Comparing the results, a couple of interesting effects are observed. First of all, the tensile strength σ_{TS} is only slightly affected with the exception of series 3B. In comparison, the 0.2% offset yield strength and the fracture strain are significantly affected after thermal exposure. In addition, the elastic moduli are also significantly affected. Fig. 6 shows the values of yield strength, tensile strength and static elastic moduli depending on the heat treatment.

When comparing the mechanical properties of the specimens heat-treated with different parameters, it becomes clear that parameters 1B and 2B have hardly any effect on the characteristic values compared to

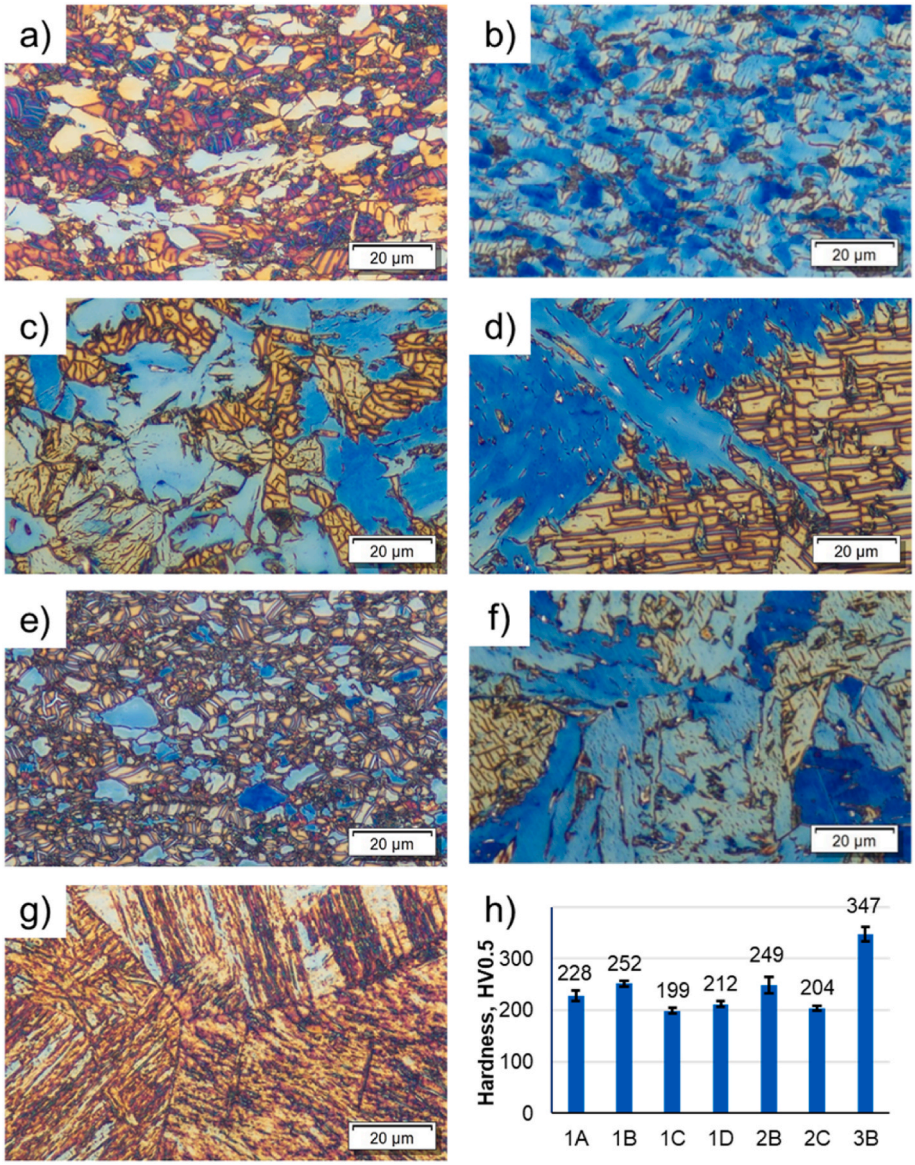

Fig. 4. Micrographs of the different heat treatment states: a) 1A, b) 1B, c) 1C, d) 1D, e) 2B, f) 2C, g) 3B, h) results of hardness measurement.

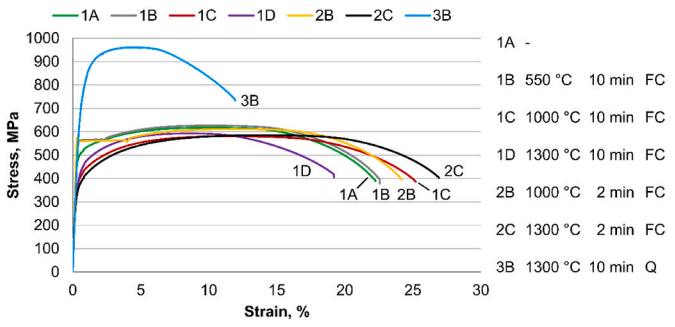

Fig. 5. Tensile test results.

the initial state (1A). Although the critical temperature range between 600 and 700 °C, as outlined in the literature, is exceeded during heat treatment 2B, the holding time is a maximum of approximately 1 min (c. f. Fig. 1), which does not result in any significant microstructural changes. Parameters 1C, 1D and 2C significantly reduce the yield strength and the elastic modulus, while the tensile strength remains almost unchanged. The yield strength after heat treatment 1C is only 75% of the original yield strength, while after 1D it is 79%, and after 2C it is 71%.

Compared to the initial state, 1C retains 77%, 1D retains 67% and 2C retains only 63% of the elastic modulus. The elastic modulus of steel is subject to change after exposure to high temperatures. As *Qiang* et al. demonstrated, the elastic modulus decreases with increasing temperature, particularly above 600 °C. It was also observed, that higher changes for high-strength steel S690 occur compared to S460 steel [4]. The extent of this change depends on exposure time, temperature range, steel grade and whether permanent microstructural changes occur.

The heat treatment parameters 3B, which result in martensitic formation, greatly increase both the yield strength (141%) and tensile strength (156%), but reduce the elastic modulus compared to the initial state (81%).

5.3. *Comparison of fatigue strength in vibration tests*

Fatigue tests were conducted in a Schenk resonance fatigue testing machine equipped with hydraulic clamps. These tests were carried out at room temperature under a constant force range, with an average fre-

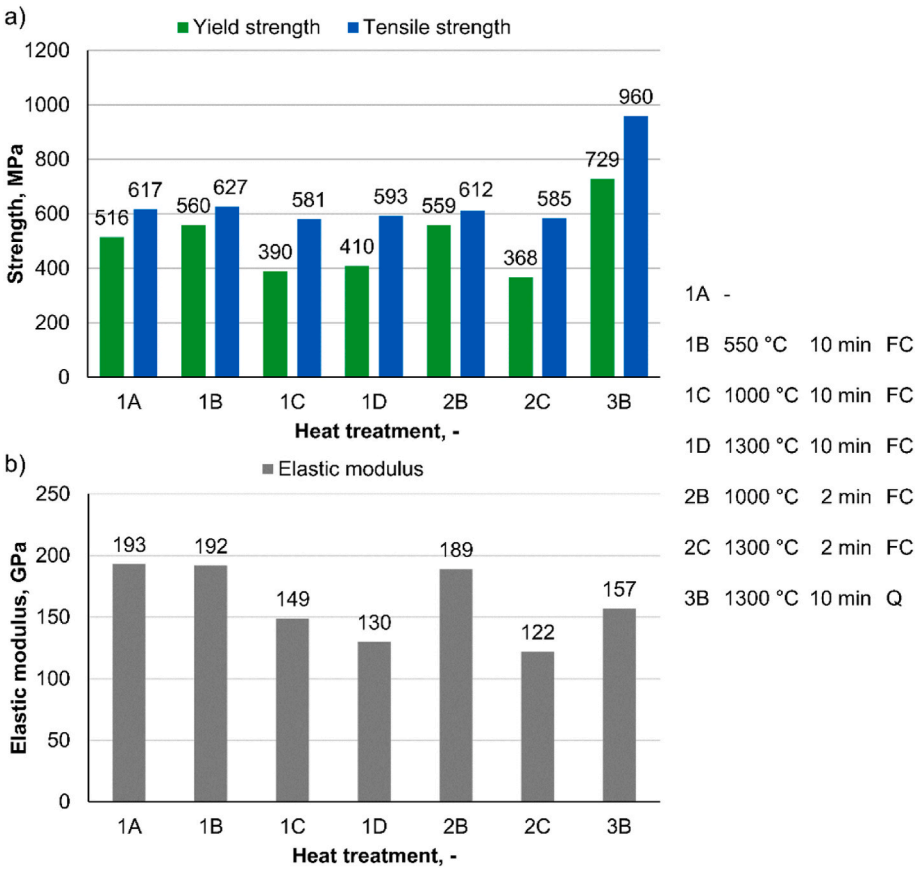

Fig. 6. Comparison of mechanical properties after heat treatments, a) yield strength and tensile strength, b) static elastic modulus, FC = free convection, Q = quenching.

quency of approximately 32 Hz. The nominal stress ratio was set to $R = 0$. Each test continued until specimen failure, with the corresponding number of cycles recorded as N. Tests were terminated at $N = 1 \cdot 10^7$ cycles. Such specimens were classified as run-outs and subsequently retested at a higher nominal stress range $\Delta\sigma$.

Based on Fig. 7, it becomes evident that the fatigue strength is influenced both by the temperature and duration of severe thermal exposure. The fatigue strength of the test series 1B and 2B is identical to the initial state (1A); however, all other states show a significant reduction in fatigue strength.

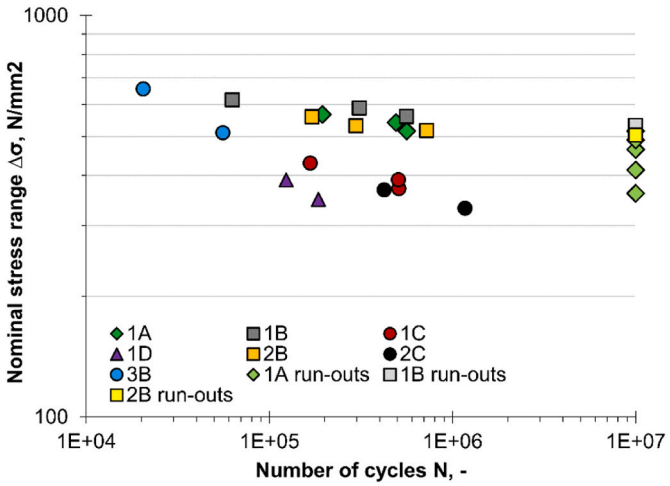

Fig. 7. Fatigue test results.

Theoretically, coarse-grained materials are more prone to fatigue crack initiation compared to fine-grained materials. Consequently, reducing grain size increases fatigue crack initiation life while simultaneously decreasing crack propagation life [49]. Microstructures with finer features demonstrate greater resistance to crack initiation than their coarser counterparts, primarily due to the higher density of slip bands [50]. In midly-notched components, as tested in the present study, the fatigue life is largely defined by crack initiation, see Ref. [48]. As the tensile strength of materials is linearly correlated to the microstructure and the fatigue crack initiation behavior [51], it is thus reasonable to assume a relation between fatigue strength of the tested specimens and their tensile strength/microstructure after thermal exposure. Thus, the fatigue test results are normalized by yield and tensile strength in Fig. 8a) and b), respectively. This is done to further analyse the effect of changing microstructures during thermal exposure on the fatigue strength.

Interestingly, normalizing by either yield or tensile strength shows different trends. While normalizing by yield strength shows a similar scatter as in the non-normalized state, normalizing by tensile strength results in a reduced scatter. This seems to be related to the fact that the thermal exposure has a different effect on yield and tensile strength. In addition, the normalized fatigue strength is quite close for all test series except for series 3B. In this case, however, the microstructure and static strength was significantly different from the other test series. This is related to the needle-like martensitic microstructure after quenching.

5.4. Interpretation and correlation of HA-EC signals

Fig. 9 shows the results of the electromagnetic testing in conjunction with the results of the mechanical test. Fig. 9a) and b) show the measured values of the amplitude of the first and third harmonics above

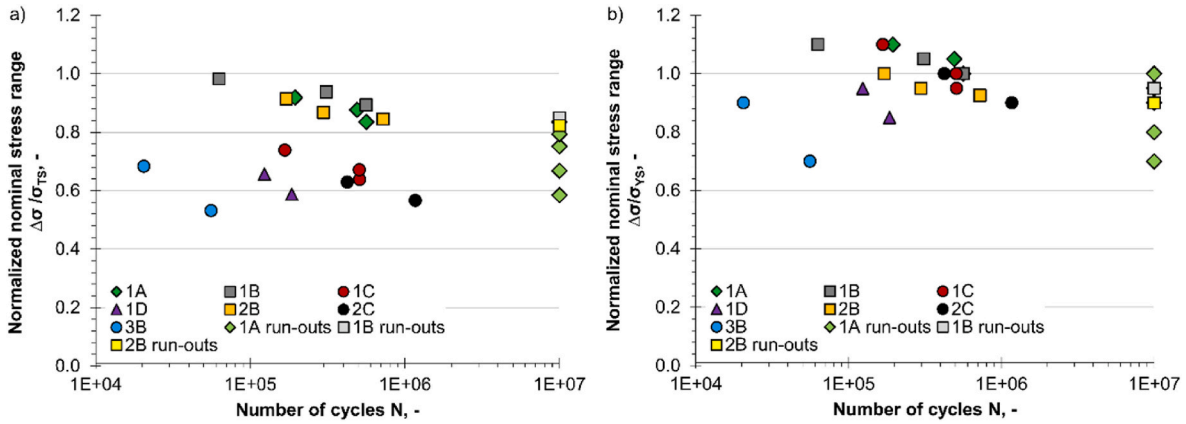

Fig. 8. Fatigue test results normalized by a) yield and b) tensile strength. For each test series the measured yield and tensile strength results from Section 5.1 were used for normalizing.

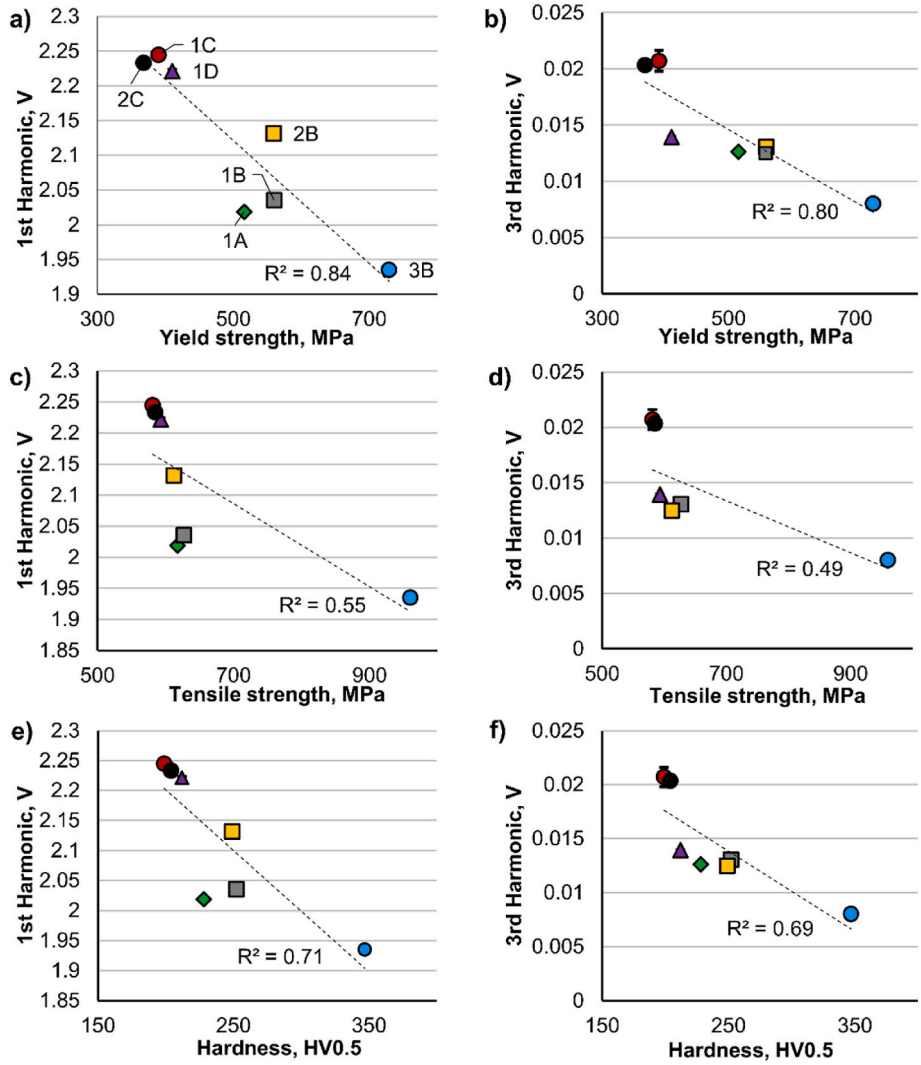

Fig. 9. a) Amplitude of 1st Harmonic vs. Yield Strength, b) Amplitude of 3rd Harmonic vs. Yield Strength, c) Amplitude of 1st Harmonic vs. Tensile Strength, d) Amplitude of 3rd Harmonic vs. Tensile Strength, e) Amplitude of 1st Harmonic vs. Hardness, f) Amplitude of 3rd Harmonic vs. Hardness.

the yield strength. An inverse linear correlation, accompanied by a high coefficient of determination, is observed between the measured values and the yield strength, for both the amplitude of the first harmonic and of the third harmonic.

A less pronounced correlation with a lower coefficient of determination can be seen in the diagrams c) to f), in which the non-destructively determined measured values are plotted against the tensile strength and hardness. Regarding diagrams c) and d), it can be seen

that heat treatment 3B results in a significantly higher tensile strength. With regard to Fig. 4g), this can be explained by the martensitic microstructure. In contrast, the other heat treatments show a linear correlation. This indicates that within a specific microstructure, in this case a ferritic-pearlitic microstructure, it is possible to make a reliable statement about the non-destructive measured values for tensile strength. Furthermore, a higher number of specimens with different properties across the entire tensile strength range should be tested and used for any regression models. A key factor is the expected cooling rate after thermal exposure. If rapid cooling by water is possible, different martensitic microstructures must be included in the regression model. On the other hand, if only air cooling is realistic, the focus should be on the ferritic-pearlitic microstructure. Regarding the elastic modulus, no correlation with the measured values could be observed.

As illustrated in diagrams e) and f), a linear relationship is evident between the amplitude of the first and third harmonic and the hardness. This correlation can be further enhanced by employing multidimensional regression models that consider multiple frequencies and harmonics components, as for example demonstrated in Ref. [45].

Fig. 10a) shows the results of the cyclic fatigue tests as a function of the heat treatment. As described in Section 5.3, heat treatments 1C, 1D, 2C and 3B significantly reduce the fatigue strength compared to the initial state. Heat treatments 1B and 2B have hardly any influence. The heat treatment states of specimens 1C, 1D, 2C and 3B differ significantly from those that exhibit fatigue strength as in the initial state.

The findings from the cyclic fatigue tests are reflected in the impedance plane of the 3rd harmonic, see Fig. 10b). The initial state 1A and the heat treatments 1B and 2B have similar physical and mechanical properties, which is why the measuring points in the impedance plane are close to each other, as highlighted by the green circle. On the other hand, changes in the microstructure due to thermal overload can be clearly distinguished from the initial state, as can be seen from the measurement points of 1C, 1D, 2C and 3B. A hard magnetic behaviour due to martensite formation at 3B leads to a lower amplitude compared to the initial state. A softer magnetic behaviour, e.g., due to coarse grain formation or a higher proportion of ferrite, leads to a higher amplitude of the 3rd harmonic.

Consequently, in the context of a feasibility study, it was successfully demonstrated that the detection of thermal damage on the exemplary S500G1+M TMCR structural steel is possible directly on the component using the HA-EC signals.

In addition to simply detecting thermal overload, harmonic analysis can be used to estimate the absolute change in yield strength, tensile strength and hardness of S500M. A similar correlation has already been successfully tested in industrial applications in steel sheet production for on-line monitoring of mechanical properties [52,53]. Consequently, the testing technique can also be used in harsh environmental conditions. Other studies on low-alloy steels have also shown that yield strength can be predicted from eddy current signals with an error of between 10 and 15% [54]. Harmonic analysis was also used to correlate the tensile strength of a car body structure after hot forming, with a deviation of only 3% [46].

With regard to the relationship between the eddy current signals and the fatigue strength of TMCR structural steels, however, further investigation is required. The results presented have shown that it is possible to qualitatively distinguish between different fatigue strengths in the impedance plane. Starting from the initial condition, three different directions can be observed in the impedance plane, see Fig. 10b). Further investigation is therefore required to determine the cause of these different positions. Moreover, the use of additional testing frequencies can be helpful, especially when setting up an AI model as part of a larger statistical validation. In addition, more detailed information about the microstructure and the electrical and magnetic properties can provide more insight into the different testing signals.

Further, it has been shown that significant thermal damage can be detected. Heat treatments in the range where microstructural changes occur also need to be investigated in more detail. With regard to the literature [1–5], temperature ranges between 600 and 700 °C with different holding times should therefore be investigated in order to examine the sensitivity of the testing technique to the slightest unwanted microstructural changes. Similarly, the question needs to be answered if the identified correlations are also present for other high-strength steels, especially if these are not thermomechanically rolled but quenched and tempered.

6. Conclusions and future work

To investigate the qualification of non-destructive electromagnetic testing technology for the detection of thermal damage, tensile and fatigue specimens of S500G1+M high-strength structural steel were subjected to various heat treatments. The resulting changes in microstructure, hardness, yield strength, tensile strength, elastic modulus, fatigue strength and electromagnetic signals were compared to the initial state. The main findings are.

- Harmonic analysis of eddy current signals can be used to detect thermal damage on S500M high-strength structural steel directly on the component.
- Thermal damage leading to reduced fatigue strength can be detected non-destructively using the impedance plane of the third harmonic.
- The amplitudes of the first and third harmonics show an inverse correlation to hardness, yield and tensile strength. This enables changes from the initial state to be detected and a statement to be

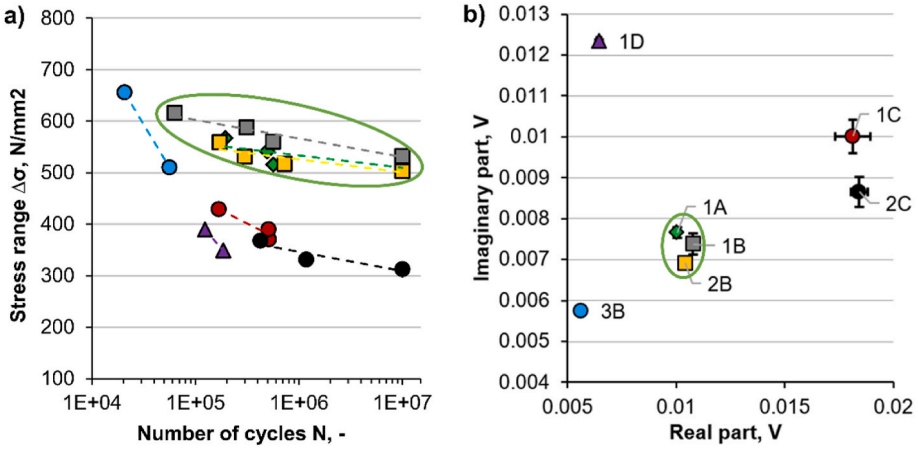

Fig. 10. a) Number of cycles vs. Stress range, b) Real part vs. Imaginary part of the 3rd Harmonic.

made about the mechanical properties that are present after thermal exposure.

Future work should focus on further qualifying the testing technology for use on real components and structures. In addition to suitable sensors, testing concepts must also be developed that are suitable for identifying suitable reference measuring points and compensating for potential interferences such as geometric influences and scaling.

CRediT authorship contribution statement

René Gansel: Data curation, Formal analysis, Investigation, Methodology, Visualization, Writing – original draft, Writing – review & editing. **Moritz Braun:** Data curation, Formal analysis, Investigation, Methodology, Visualization, Writing – original draft, Writing – review & editing. **Sören Ehlers:** Resources, Supervision, Writing – review & editing. **Sebastian Barton:** Data curation, Methodology, Visualization, Supervision, Writing – review & editing.

Declaration of competing interest

The authors declare that they have no known competing financial interests or personal relationships that could have appeared to influence the work reported in this paper.

Acknowledgements

The authors thank Dillinger Hütte for providing the S500G1+M steel.

References

[1] Saedi Daryan A, Barzvar H, Fakharzadeh Naeini E, Ketabdari H. Post-fire performance of butt-welded connections in ST-37 steel. Fire Technol 2023;59(2):691–711. https://doi.org/10.1007/s10694-023-01362-2.
[2] Kang L, Wu B, Liu X, Ge H. Experimental study on post-fire mechanical performances of high strength steel Q460. Adv Struct Eng 2021;24(12):2791–808. https://doi.org/10.1177/13694332211010601.
[3] Zeybek Ö, Polat V, Özkılıç YO. The response of high strength S700 MC steel after fire exposure. J Constr Steel Res 2024;219:1–12. https://doi.org/10.1016/j.jcsr.2024.108790.
[4] Qiang X, Bijlaard FS, Kolstein H. Post-fire mechanical properties of high strength structural steels S460 and S690. Eng Struct 2012;35:1–10. https://doi.org/10.1016/j.engstruct.2011.11.005.
[5] Wang X-Q, Tao Z, Hassan MK. Post-fire behaviour of high-strength quenched and tempered steel under various heating conditions. J Constr Steel Res 2020;164:1–17. https://doi.org/10.1016/j.jcsr.2019.105785.
[6] Dowling NE. Mechanical behavior of materials: engineering methods for deformation. Fracture, and fatigue, vol. 4. Pearson; 2013.
[7] Ritchie RO. Mechanisms of fatigue-crack propagation in ductile and brittle solids. Int J Fract 1999;100(1):55–83. https://doi.org/10.1023/A:1018655917051.
[8] Lippold JC, Kotecki DJ. Welding metallurgy and weldability of stainless steels. Wiley; 2005.
[9] Suresh S. Fatigue of materials. 2. ed. Cambridge Univ. Pr: Cambridge; 1998.
[10] Paul VT, Saroja S, Vijayalakshmi M. Microstructural stability of modified 9Cr–1Mo steel during long term exposures at elevated temperatures. J Nucl Mater 2008;378(3):273–81. https://doi.org/10.1016/j.jnucmat.2008.06.033.
[11] Buchmayr B. Thermomechanical treatment of steels - a real disruptive technology since decades. Steel Res Int 2017;88(10):1–14. https://doi.org/10.1002/srin.201700182.
[12] Liang X, DeArdo AJ. A study of the influence of thermomechanical controlled processing on the microstructure of bainite in high strength plate steel. Metall Mater Trans 2014;45(11):5173–84. https://doi.org/10.1007/s11661-014-2444-5.
[13] Fleischer RL. High-strength, high-temperature intermetallic compounds. J Mater Sci 1987;22(7):2281–8. https://doi.org/10.1007/BF01082105.
[14] Wang J, Chen Y, Zuo L, Zhao H, Ma N. Evaluation of thermal fatigue life and crack morphology in brake discs of low-alloy steel for high-speed trains. Materials 2022;15(19):1–15. https://doi.org/10.3390/ma15196837.
[15] Ghafouri M, Amraei M, Pokka A-P, Björk T, Larkiola J, Piili H, Zhao X-L. Mechanical properties of butt-welded ultra-high strength steels at elevated temperatures. J Constr Steel Res 2022;198:1–13. https://doi.org/10.1016/j.jcsr.2022.107499.
[16] Brnic J, Brcic M, Balos S, Vukelic G, Krscanski S, Milutinovic M, Dramicanin M. S235JRC+C steel response analysis subjected to uniaxial stress tests in the area of high temperatures and material fatigue. Sustainability 2021;13(10):1–16. https://doi.org/10.3390/su13105675.
[17] Neuenschwander M, Scandella C, Knobloch M, Fontana M. Modeling elevated-temperature mechanical behavior of high and ultra-high strength steels in structural fire design. Mater Des 2017;136:81–102. https://doi.org/10.1016/j.matdes.2017.09.041.
[18] Li G-Q, Song L-X. Mechanical properties of TMCP Q690 high strength structural steel at elevated temperatures. Fire Saf J 2020;116:1–7. https://doi.org/10.1016/j.firesaf.2020.103190.
[19] Pandey M, Young B. Post-fire mechanical response of high strength steels. Thin-Walled Struct 2021;164:1–30. https://doi.org/10.1016/j.tws.2021.107606.
[20] Azhari F, Heidarpour A, Zhao X-L. On the use of Bernstain-Bézier functions for modelling the post-fire stress-strain relationship of ultra-high strength steel (Grade 1200). Eng Struct 2018;175:605–16. https://doi.org/10.1016/j.engstruct.2018.08.088.
[21] Gyura L, Gáspár M, Balogh A. The effect of flame straightening on the microstructure and mechanical properties of different strength steels. Weld World 2021;65(3):543–60. https://doi.org/10.1007/s40194-020-01055-2.
[22] Lacalle R, Álvarez JA, Ferreño D, Portilla J, Ruiz E, Arroyo B, Gutiérrez-Solana F. Influence of the flame straightening process on microstructural, mechanical and fracture properties of S235 JR, S460 ML and S690 QL structural steels. Exp Mech 2013;53(6):893–909. https://doi.org/10.1007/s11340-013-9723-8.
[23] Pattee HE, Evans RM, Monroe RE. Flame straightening and its effect on base metal properties, No. SSC-198 Summ Rpt. 1969.
[24] Hanus F, Hubo R. Flame straightening of thermomechanically rolled structural steel. Steel Res 1999;70(4–5):193–7. https://doi.org/10.1002/srin.199905625.
[25] Chen J, Ji D-M, Cai X, Wang D, Dai C, Wang J. Effect of holding duration at maximum and minimum stress on creep fatigue interaction of P92 steel. Materials at High Temperatures 37 2020;1:51–60. https://doi.org/10.1080/09603409.2019.1693141.
[26] Rémy L. Thermal-mechanical fatigue (including thermal shock). In: Comprehensive structural integrity. second ed. 2023.
[27] Hua J, Wang F, Xue X, Ding Z, Sun Y, Xiao L. Ultra-low cycle fatigue performance of Q690 high-strength steel after exposure to elevated temperatures. J Build Eng 2022;57:1–18. https://doi.org/10.1016/j.jobe.2022.104832.
[28] Hua J, Yang Z, Zhou F, Hai L, Wang N, Wang F. Effects of exposure temperature on low–cycle fatigue properties of Q690 high–strength steel. J Constr Steel Res 2022;190:1–12. https://doi.org/10.1016/j.jcsr.2022.107159.
[29] Franclois M, Rémy L. Thermal-mechanical fatigue of MAR-M 509 superalloy. Comaprison with low-cycle fatigue behaviour. Fatig Fract Eng Mater Struct 1991;14(1):115–29. https://doi.org/10.1111/j.1460-2695.1991.tb00647.x.
[30] Ji D, Zhang L-C, Ren J, Wang D. Creep-fatigue interaction and cyclic strain analysis in P92 steel based on test. J Mater Eng Perform 2015;24(4):1441–51. https://doi.org/10.1007/s11665-015-1446-9.
[31] Coffin LF. Fatigue at high temperature-prediction and interpretation. Proc Inst Mech Eng 1974;188(1):109–27. https://doi.org/10.1243/PIME_PROC_1974_188_014_02.
[32] Kang HT, Lee Y-L, Chen J, Fan D. A thermo-mechanical fatigue damage model for variable temperature and loading amplitude conditions. Int J Fatig 2007;29:1797–802. https://doi.org/10.1016/j.ijfatigue.2007.03.008. 9-11.
[33] Guo Y, Fang C, Zheng Y. Post-fire hysteretic and low-cycle fatigue behaviors of Q345 carbon steel. J Constr Steel Res 2021;187:1–18. https://doi.org/10.1016/j.jcsr.2021.106991.
[34] Bernard M, Scheer C, Böhm V, Reimche W. New developments in non-destructive testing for quality assurance in component manufacturing. Steel Res Int 2009;80(12):916–28. https://doi.org/10.2374/SRI09SP144.
[35] Mróz G, Reimche W, Frackowiak W, Bruchwald O, Maier HJ. Setting discrete yield-stress sensors for recording early component loading using eddy-current array technology and induction thermography. Procedia Technology 2014;15:484–93. https://doi.org/10.1016/j.protcy.2014.09.008.
[36] Barton S, Reimche W, Maier HJ. Three-dimensional data storage in the subsurface region and fast read-out technologies for determining the mechanical load history of components. HTM Journal of Heat Treatment and Materials 2018;73(1):13–26. https://doi.org/10.3139/105.110343.
[37] Fricke LV, Thürer SE, Jahns M, Breidenstein B, Maier HJ, Barton S. Non-destructive, contactless and real-time capable determination of the α'-martensite content in modified subsurfaces of AISI 304. J Nondestruct Eval 2022;41(4):1–13. https://doi.org/10.1007/s10921-022-00905-x.
[38] Gansel R, Quanz M, Lohrengel A, Maier HJ, Barton S. Qualification of austenitic stainless steels for the development of load-sensitive material sensors. J Mater Eng Perform 2024:1–13. https://doi.org/10.1007/s11665-024-09287-9.
[39] Mercier D, Lesage J, Decoopman X, Chicot D. Eddy currents and hardness testing for evaluation of steel decarburizing. NDT E Int 2006;39(8):652–60. https://doi.org/10.1016/j.ndteint.2006.04.005.
[40] Chan SC, Grimberg R, Hejase JA, Zeng Z, Lekeakatakunju P, Udpa L, Udpa SS. Nonlinear eddy current technique for characterizing case hardening profiles. IEEE Trans Magn 2010;46(6):1821–4. https://doi.org/10.1109/tmag.2010.2044980.
[41] Reimche W, Zwoch S, Bruchwald O, Bach F-W, Klümper-Westkamp H, Lütjens J, Zoch H-W. Hochtemperatur Prüftechnik ermöglicht Einblicke in die Werkstoffumwandlung und Phasenausbildung bei Hochleistungsbauteilen. e-Journal of Nondestructive Testing 2012;17:1–12. 05.
[42] Bruchwald O, Frackowiak W, Reimche W, Maier HJ. Non-destructive in situ monitoring of the microstructural development in high performance steel components during heat treatment. La Metall Ital 2015;11(12):29–37.
[43] Gansel R, Zimmermann C, Fricke LV, Lüdtke M, Klümper-Westkamp H, Fechte-Heinen R, Maier HJ, Zaremba D. Characterization of graded subsurface zones in industrial case-hardening using a non-destructive testing system. HTM Journal of

Heat Treatment and Materials 2021;76(3):237–45. https://doi.org/10.1515/htm-2021-0006.
[44] Stegemann D, Reimche W, Feiste KL, Reichert C, Marques-Fetter P. Determination of hardness and hardness penetration depth of metal components by Non Linear Harmonics Analysis. AIP Conf Proc 1999;497(1):228–34. https://doi.org/10.1063/1.1302008.
[45] Bach F-W, Martin B, Reimche W. Nondestructive in-process determination of hardness values by harmonic analysis of eddy current signals. e-Journal of Nondestructive Testing 2006;11(11):1–12.
[46] Chojecki H, Nehring J, Engels H, Müller-Bollenhagen C. Ermittlung mechanisch-technologischer Eigenschaften warmumgeformter Automobilstrukturen durch die magnet-induktive Oberwellenanalyse. e-Journal of Nondestructive Testing 2007;12(12):1–13.
[47] ISO. EN ISO 6892-1:2016 - Metallic materials – Tensile testing – Part 1: Method of test at room temperature 2016.
[48] Braun M, Fischer C, Baumgartner J, Hecht M, Varfolomeev I. Fatigue crack initiation and propagation relation of notched specimens with welded joint characteristics. Metals 2022;12(4):1–24. https://doi.org/10.3390/met12040615.
[49] Braun M, Chen T, Shen J, Fassmer H, Klusemann B, Sheikhi S, Ehlers S, Müller E, Sarmast A, Schubnell J. Fatigue crack initiation and propagation in plain and notched PBF-LB/M, WAAM, and wrought 316L stainless steel specimens. Mater Des 2024;244:1–18. https://doi.org/10.1016/j.matdes.2024.113122.
[50] Chan KS. Roles of microstructure in fatigue crack initiation. Int J Fatig 2010;32(9):1428–47. https://doi.org/10.1016/j.ijfatigue.2009.10.005.
[51] Pavlina EJ, van Tyne CJ. Correlation of yield strength and tensile strength with hardness for steels. J Mater Eng Perform 2008;17(6):888–93. https://doi.org/10.1007/s11665-008-9225-5.
[52] Heutling B, Reimche W, Krys A, Grube L, Stock M, Bach F-W, Kroos J, Stolzenberg M, Westkämper G. Online NDE of mechanical-technological material characteristics of cold rolled steel strips by using the harmonic analysis of eddy current signals. Int J Appl Electromagn Mech 2004;19(1–4):445–51. https://doi.org/10.3233/JAE-2004-606.
[53] Heingärtner J, Born M, Hora P. Online acquisition of mechanical material properties of sheet metal for the prediction of product quality by eddy current. 10th European conference on non-destructive testing (ECNDT 2010). 2010. p. 1–7.
[54] Li K, Qiu P, Wang P, Lu Z, Zhang Z. Estimation method of yield strength of ferromagnetic materials based on pulsed eddy current testing. J Magn Magn Mater 2021;523:1–9. https://doi.org/10.1016/j.jmmm.2020.167647.